KURENAI

Kyoto University Research Information Repository

KYOTO UNIVERSITY

Title	Large-strain-induced magnetic properties of Co electrodeposited on nanoporous Au
Author(s)	Hakamada, Masataka; Hirashima, Fumi; Takahashi, Masaki; Nakazawa, Takumi; Mabuchi, Mamoru
Citation	Journal of Applied Physics (2011), 109(8)
Issue Date	2011-04
URL	http://hdl.handle.net/2433/141813
Right	© 2011 American Institute of Physics
Type	Journal Article
Textversion	publisher

Kyoto University

Large-strain-induced magnetic properties of Co electrodeposited on nanoporous Au

Masataka Hakamada,[a)] Fumi Hirashima, Masaki Takahashi, Takumi Nakazawa, and Mamoru Mabuchi

Department of Energy Science and Technology, Graduate School of Energy Science, Kyoto University, Yoshidahonmachi, Sakyo, Kyoto 606-8501, Japan

Nanostructured Co with large lattice extension and contraction was produced by electrodepositing Co on nanoporous Au. The Co deposited showed a low magnetic saturation of 76 emu/g and a high coercivity of 462 Oe. First-principles calculations showed that the magnetic moment of a Co atom is significantly decreased by lattice contraction. Therefore, the noteworthy magnetic properties of the Co deposited are attributed to the large lattice strain. Also, molecular dynamics simulation showed that the lattice extension and contraction of about 10% are generated in the overall Co crystal. This is in agreement with the experimental results of HRTEM observation. The constraint of the movement of Co atoms by the concave structure of nanoporous Au leads to a wide spread of large strain region. © *2011 American Institute of Physics*. [doi:10.1063/1.3575327]

I. INTRODUCTION

Magnetic nanostructured materials such as Co nanoparticles are of great interest for a variety of applications in such as sensors, actuators, and magnetic data storage devices because these materials have excellent remarkable magnetic properties such as high magnetic anisotropy, superparamagnetism, and enhanced magnetic saturation.[1–3] These outstanding magnetic properties of nanostructured materials result from finite-size effects and surface effects. The finite-size effects are due to the quantum confinement of electrons, and the single-dominant state and the superparamagnetic state are typical of finite-size effects. For a spherical particle, the critical diameter below which a single-domain state is attained is about 10 nm for Co.[3] Hence, very high coercivity can be obtained in Co nanoparticles of 10 nm diameter. In addition, when the diameter becomes much smaller than the critical size, the thermal energy exceeds the energy barrier for spin rotation, resulting in a superparamagnetic state. On the other hand, the surface effects result from the breaking of the symmetry of the crystal structure. In the nanostructured materials, the symmetry breaking occurs at numerous sites such as at the interfaces, free surfaces and grain boundaries. This local breaking of symmetry gives rise to band narrowing and spin disorder. The band narrowing enhances the magnetic moment,[4–7] whereas the spin disorder reduces the magnetic moment[2,3] and enhances the magnetic anisotropy.[8–11] To date, we have gained a deep understanding on the finite-size effects and surface effects having complicated effects on the magnetic properties of nanostructured materials.

Nanoporous metals, which are produced by selective electrochemical dealloying of more active components in a homogeneous alloy,[12] are one of the interesting nanostructured materials. Recently, it has been found that nanoporous Ni exhibits unique magnetic properties owing to the surface effects and the large lattice strain.[13,14] The strain effects have also been found in other nanostructured materials.[15–18] Thus, the magnetic properties of nanostructured materials are strongly affected by strain as well as the size effect because large strain is often generated in nanostructured materials. However, an understanding of the strain effects is still lacking for nanostructured materials.

In this work, nanostructured Co is produced by electrodepositing Co on nanoporous Au, and its magnetic properties are investigated using a vibration sample magnetometer. Bimetallic nanoparticles exhibit an interaction between the core metal and the shell metal.[19,20] In the Co electrodeposited on nanoporous Au, large strain is expected to be generated because of Co/Au interaction. In the present work, molecular dynamics (MD) simulations and first-principles calculations are performed to investigate the origin of strain generation and the effects of strain on the magnetic moment.

II. EXPERIMENTAL AND SIMULATION METHODS

Au (>99.9 mass%) and Ag (>99.9 mass %) ingots were arc-melted together in Ar atmosphere to prepare a precursor $Au_{0.35}Ag_{0.65}$ ingot. After homogenization at 1173 K for 24 h in Ar atmosphere and subsequent cold rolling, nanoporous Au was synthesized by dealloying of the alloy (free corrosion) at 263 K for 15 h in 70 mass % HNO_3. A scanning electron micrograph of the nanoporous Au is shown in Fig. 1. The average ligament and pore diameters were 7.4 and 21 nm, respectively.

Co was electrodeposited on the nanoporous Au for 1 s. The electrolyte composition was $CoSO_4 \cdot 7H_2O$ (0.5 mol/l). The pH of the electrolyte was adjusted to 3.0 using H_2SO_4. Working electrodes consisted of 5-mm-diameter nanoporous Au. A Cu wire fitted around the edge of the nanoporous Au served as the electrical contact during deposition. The counterelectrode was a platinum wire. The current density was

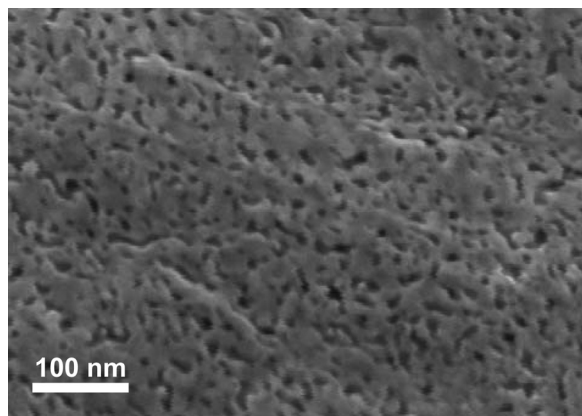a)Author to whom correspondence should be addressed. Electronic mail: hakamada.masataka.3x@kyoto-u.ac.jp.

FIG. 1. Scanning electron micrograph of nanoporous Au. The average ligament and pore diameters are 7.4 and 21 nm, respectively.

170 mA/cm^2 with direct current. The bath temperature was maintained at 303 K.

Microstructures of the Co deposited were investigated using a high-resolution transmission electron microscope (HRTEM). In addition, elemental analysis was performed by energy dispersive x-ray spectrometry (EDS) coupled with HRTEM. The magnetization hysteresis loop was recorded at room temperature at a maximum applied field of 10 kOe using a vibration sample magnetometer.

The framework of the density functional theory with the CASTEP code was adopted to investigate the effects of lattice strain on the magnetic moment of Co.[21] Infinite lattice systems for *fcc* and *hcp* phases of Co were modeled using periodic boundary conditions, where the lattice parameter was changed in the strain range from −20 to +25%. The code was, therefore, ideally suitable for calculations of periodic systems. The exchange-correlation interactions were treated using the spin-polarized version of the generalized gradient approximation within the Perdew-Burke-Ernzerhof scheme.[22] The valence electrons described by Vanderbilt-type nonlocal ultrasoft pseudopotentials are Co 3d^{7}4s.[2] Ultrasoft pseudopotentials represented in reciprocal space were used for all elements in our calculations. The self-consistent electronic minimization based on density mixing was performed until the convergence criterion was satisfied, that is, 5.0×10^{-6} eV for the energy change per atom. The cutoff energy was set to be 330 eV for all models. The Brillouin zone was sampled using a $15 \times 15 \times 15$ Monkhorst-Pack mesh of *k* points for the *fcc* phase and $14 \times 14 \times 8$ Monkhorst-Pack mesh of *k* points for the *hcp* phase. Mulliken populations were employed to obtain the magnetic moment per atom. The calculations on the magnetic moments were performed at 0 K.

Also, a MD simulation was performed on a Co-deposition model where an *fcc* Co crystal was deposited on concave *fcc* Au, where the *x*-direction (misorientation axis) was [1$\bar{1}$0], the *y*-direction was [11$\bar{2}$] and the *z*-direction was [111] to investigate the origin of strain generation in the Co deposited [Fig. 7(a)]. The dimensions of the model unit were 1.4 nm long (*x*-direction), 10 nm wide (*y*-direction) and 10 nm high (*z*-direction). A periodic boundary condition was applied to the *x*- and *y*-directions. In the *z*-direction, the top and bottom layers of Au were fixed to prevent the concave profile from

moving, which fitted the present experiment. To ensure the stability of the structure, a relaxation calculation was carried out for 10 ps at 298 K with an NTV ensemble (where N (number of atoms), T (temperature) and V (volume of the cell) are constant). In the simulation, the generalized EAM potential was used to describe the Co-Co, Co-Au, and Au-Au interatomic interactions.[23] The potential enables the calculation to be performed for an alloy containing Co and Au.

III. RESULTS AND DISCUSSION

A TEM image of the cross section of the Co deposited is shown Fig. 2. It can be seen that many pore spaces are filled [Fig. 2(a)]. The EDS analysis at the filled spot revealed that Co atoms filled the pore spaces. It was impossible to clarify the crystal phase of the Co deposited from the EDS result. The stable crystal phase of Co depends on the size; for example, for Co nanoparticles, the stable phase is an *fcc* phase for diameter <20 nm, an *hcp* phase for diameter >40 nm, and a mixture of *fcc* and *hcp* phases for a diameter of approximately 30 nm.[24] The average pore diameter was 21 nm for nanoporous Au, and therefore, the phase of Co deposited may be a mixture of *fcc* and *hcp* phases.

A HRTEM image of the Co deposited is shown in Fig. 3. An inspection of HRTEM images revealed that the lattice spacing of the Co deposited significantly varied; for example, the lattice spacings were 0.257 nm at the left middle point, 0.231 nm at the middle lower point, and 0.187 nm at the right upper point, although it was impossible to identify the crystal plane because the diffraction pattern was too complicated. In the case of no strain, the maximum lattice spacings were 0.204 nm for the (111) plane in *fcc* Co and 0.216 nm for the (10$\bar{1}$0) plane in *hcp* Co. Note that the lattice
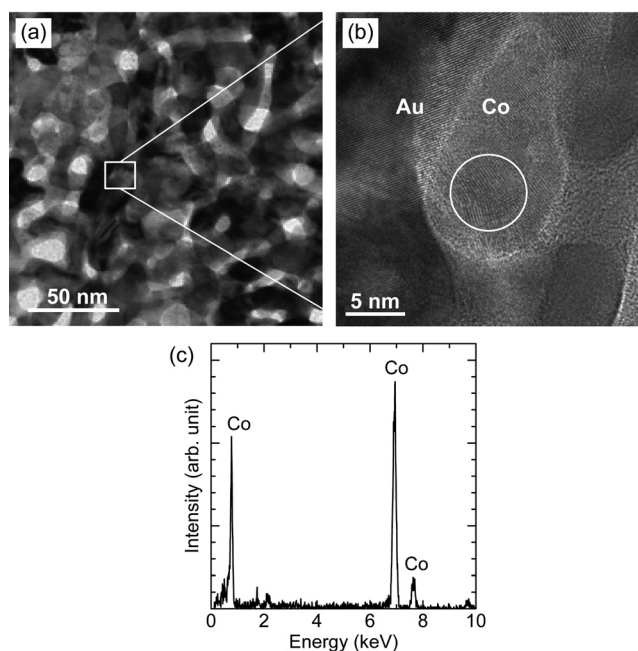

FIG. 2. (a) Transmission electron microscopy (TEM) image of the cross section of the Co deposited on nanoporous Au, (b) enlarged TEM image of the area within the white square in (a), and (c) energy-dispersed x-ray spectrograph of area within the white circle in (b). The pore spaces are filled with Co crystals.
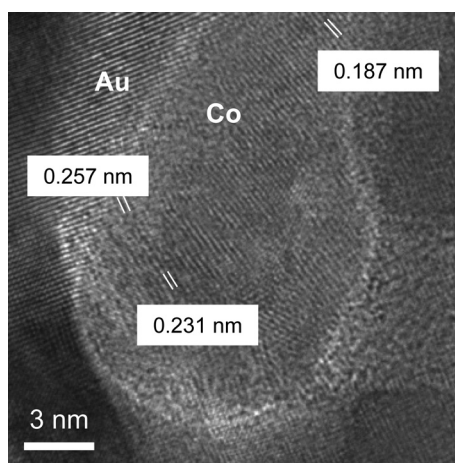
FIG. 3. High-resolution transmission electron microscope image of the Co deposited on nanoporous Au. Note that significantly large lattice strain is generated upon lattice extension and contraction in the deposited Co.

FIG. 5. Variation in magnetic moment of Co atom as a function of the lattice strain, as determined by first-principles calculations. Note that the magnetic moment is significantly decreased by lattice contraction in the strain range of more than 5% for fcc and 10% for hcp, whereas the moment is gradually increased by lattice extension in both cases of fcc and hcp.

spacing of 0.257 nm at the left middle point in Fig. 3 is much larger than the lattice spacing in the case of no strain. By comparison with the lattice spacing for the (111) plane of *fcc* Co and the $(10\bar{1}0)$ plane of *hcp* Co, the lattice strain at the left middle point is calculated to be +25% for *fcc* Co and +19% for *hcp* Co, the lattice strain at the middle lower point is calculated to be +13% for *fcc* Co and +7% for *hcp* Co, and the lattice strain at the right upper point is calculated to be −8% for *fcc* Co and −13% for *hcp* Co. Thus, significantly large lattice strains were generated in the Co deposited.

Figure 4 shows the magnetization hysteresis loop of the Co deposited. The Co deposited showed the magnetic saturation of 76 emu/g and the coercivity of 462 Oe. The magnetic saturation of 76 emu/g is lower than that for bulk Co (= 162 emu/g) and the coercivity of 462 Oe is larger than that for bulk Co (= 10 Oe). The lattice strains in the Co deposited are significantly larger than those of Co epitaxially deposited on flat Au substrate with no curvature.[25] Therefore, the low magnetic saturation and high coercivity of the Co deposited are likely to be attributed to the large strain.

The effects of lattice strain on the magnetic moment of a Co atom were elucidated by the first-principles calculations. The results are shown in Fig. 5. Note that the magnetic moment is significantly decreased by lattice contraction, in particular, in the strain range of more than 5% for *fcc* and 10% for *hcp*, whereas the moment is gradually increased by lattice extension in both cases of *fcc* and *hcp*. Bond narrowing is responsible for the enhanced moment by lattice extension, and bond broadening gives rise to the reduced moment by lattice contraction, as shown in Fig. 6. Therefore, the large contraction strain is likely to be responsible for the low magnetic saturation of the Co deposited.
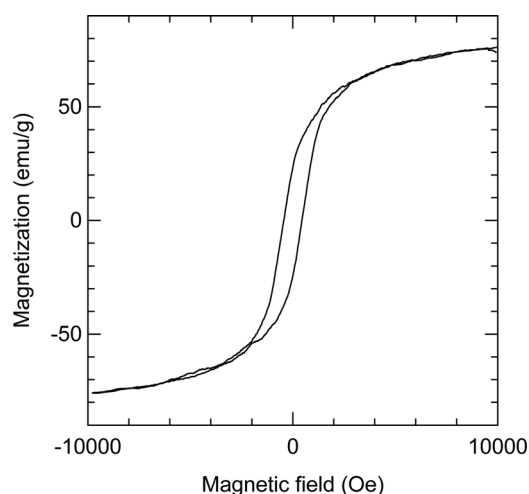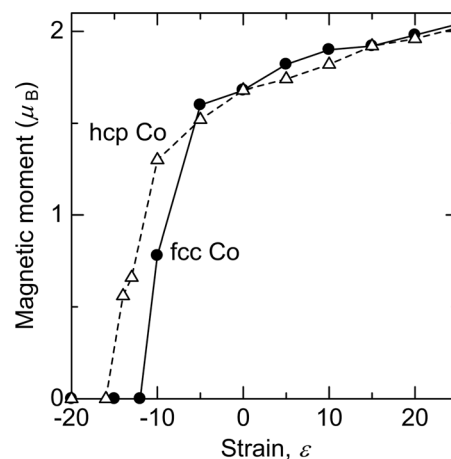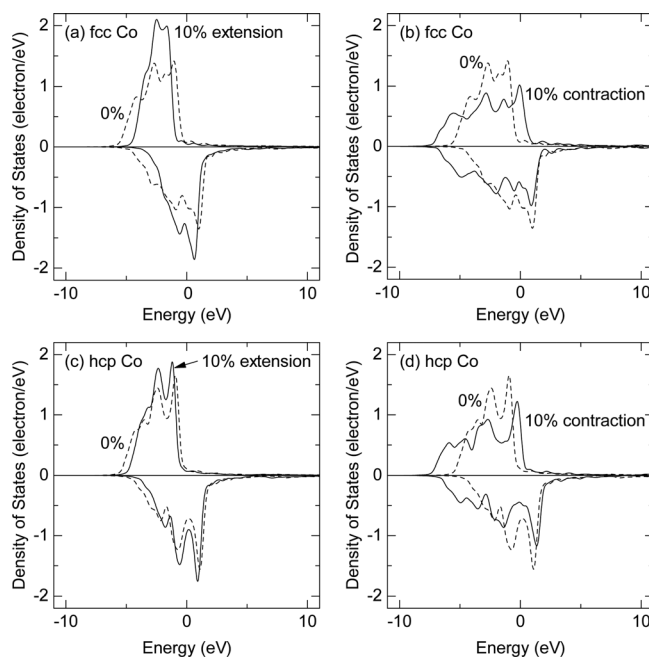

FIG. 4. Magnetization hysteresis loop of the Co deposited on nanoporous Au. The Co deposited showed the magnetic saturation of 76 emu/g and the coercivity of 462 Oe.

FIG. 6. Partial density of states of 3d orbital in Co atom with and without lattice strain: (a) 10% extension for fcc Co, (b) 8% contraction for fcc Co, (c) 20% extension for hcp Co, and (d) 13% contraction for hcp Co. Fermi level is defined as zero energy.
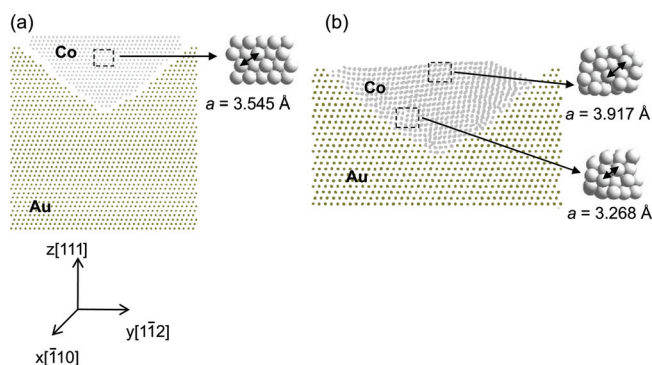
FIG. 7. (Color online) Atomic geometry in the model where an fcc Co crystal is deposited on concave fcc Au: (a) before the relaxation calculation and (b) after the relaxation calculation. Lattice extension and contraction of about 8–10% are generated in the overall Co crystal.

The high coercivity results from the enhanced magnetic anisotropy. In general, the magnetic anisotropy can be divided into magnetocrystalline anisotropy, magnetoelastic anisotropy, shape anisotropy, externally induced anisotropy, and exchange anisotropy. Moreover, in nanostructured materials, the surface spin disorder enhances the anisotropy.[8–11] The magnetocrystalline and magnetoelastic anisotropies are due to spin-orbit coupling and the shape anisotropy is of dipolar origin. The lattice strain can contribute to the enhancement of anisotropy through magnetoelasitc coupling. Therefore, the high coercivity in the Co deposited is due to not only the surface spin disorder, but also the large lattice strain. In the present work, the first-principles calculations were performed at 0 K. Recently, Šipr *et al.*[26] investigated the temperature dependence of the average magnetic moment of free Fe clusters consisting of 9–89 atoms, and they showed that the average magnetic moment at 300 K is almost the same as that at 0 K. Therefore, the results obtained in the present work are valid in the temperature range of 0–300 K.

In the present work, we demonstrated that the Co deposited exhibits large lattice extension and contraction, resulting in low magnetic saturation and high coercivity. Allenspach *et al.*[25] investigated the strain in an epitaxial Co/Au film and they showed that a large tensile strain of 14% was generated at the first layer owing to lattice mismatch, but the strain disappeared at the sixth layer. It is of interest to note that large lattice strain was generated in the overall Co deposited in the present work. The results of MD simulation using the model in which the Co atoms are deposited on concave Au are shown in Fig. 7. Lattice extension and contraction of approximately 8–10% are generated in the overall Co crystal. This is in agreement with the experimental results of HRTEM observation. Such large strain was not found in the previous works in which Co deposited on a flat and planar substrate was investigated.[27,28] The constraint of the movement of Co atoms by the concave structure of nanoporous Au leads to a wide spread of large strain region in the deposited Co.

IV. CONCLUSIONS

Nanostructured Co was produced by electrodepositing Co on nanoporous Au. HRTEM observation revealed that

large lattice strain was generated upon lattice extension and contraction in the Co deposited.

The Co deposited showed a low magnetic saturation of 76 emu/g and a high coercivity of 462 Oe. The first-principles calculation showed that the magnetic moment is significantly decreased by lattice contraction. Also, the lattice strain contributes to the enhanced anisotropy through magnetoelasitc coupling. Therefore, the large strain is responsible for the low magnetic saturation and high coercivity of the Co deposited.

The MD simulation using the model where the Co atoms are deposited on concave Au showed that the lattice extension and contraction of about 8–10% are induced in the overall Co crystal. This is in agreement with the experimental results of HRTEM observation. The constraint of the movement of Co atoms by the concave structure of nanoporous Au leads to a wide spread of large strain region.

[1]D. Sander, J. Phys.: Condens. Matter **16**, R603 (2004).
[2]X. Batlle and A. Labarta, J. Phys. D: Appl. Phys. **35**, R15 (2002).
[3]A.-H. Li, E. L. Salabas, and F. Schüth, Angew. Chem. Int. Ed. **46**, 1222 (2007).
[4]F. Li, M. R. Press, S. N. Khanna, and P. Jena, Phys. Rev. B **39**, 6914 (1989).
[5]R. H. Kodama, J. Magn. Magn. Mater. **200**, 359 (1999).
[6]M. Respaud, J. M. Broto, H. Rakoto, A. R. Fert, L. Thomas, B. Barbara, M. Verelst, E. Snoeck, P. Lecante, A. Mosset, J. Osuna, T. O. Ely, C. Amiens, and B. Mosset, Phys. Rev. B **57**, 2925 (1998).
[7]I. M. L. Billas, A. Châtelain, and W. A. de Heer, Science **265**, 1682 (1994).
[8]Ò. Iglesias and A. Labarta, Phys. Rev. B **63**, 184416 (2001).
[9]D. A. Dimitrov and G. M. Wysin, Phys. Rev. B **50**, 3077 (1994).
[10]D. A. Dimitrov and G. M. Wysin, Phys. Rev. B **51**, 11947 (1995).
[11]R. H. Kodama and A. E. Berkowitz, Phys. Rev. B **59**, 6321 (1999).
[12]J. Erlebacher, M. J. Aziz, A. Karma, N. Dimitrov, and K. Sieradzki, Nature **410**, 450 (2001).
[13]M. Hakamada, M. Takahashi, T. Furukawa, and M. Mabuchi, Appl. Phys. Lett. **94**, 153105 (2009).
[14]M. Hakamada, M. Takahashi, T. Furukawa, and M. Mabuchi, Phil. Mag. **90**, 1915 (2010).
[15]M. Yuasa, K. Kajikawa, M. Hakamada, and M. Mabuchi, Appl. Phys. Lett. **95**, 162502 (2009).
[16]B. Schulz and K. Baberschke, Phys. Rev. B **50**, 13467 (1994).
[17]J. Lee, G. Lauhoff, M. Teselepi, S. Hope, P. Rosenbush, J. A. C. Bland, H. A. Dürr, G. van der Laan, J. P. Schillé, and J. D. Matthew, Phys. Rev. B **55**, 15103 (1997).
[18]B. H. Liu and J. Ding, Appl. Phys. Lett. **88**, 042506 (2006).
[19]N. S. Sobal, M. Hilgendorff, H. Môhwald, M. Giersig, M. Spasova, T. Radetic, and M. Faele, Nano Lett. **2**, 621 (2002).
[20]O. Crisan, M. Angelakeris, K. Simeonidis, Th. Kehagias, Ph. Komninou, M. Giersig, and N. K. Flevaris, Acta Mater. **54**, 5251 (2006).
[21]M. C. Payne, M. P. Teter, D. C. Allan, T. A. Arians, and J. D. Joannopoulos, Rev. Mod Phys. **64**, 1045 (1992).
[22]J. P. Perdew, K. Burke, and M. Ernzerhof, Phys. Rev. Lett. **77**, 3865 (1996).
[23]X. W. Zhow, H. N. G. Wandley, R. A. Johnson, D. J. Larson, N. Tabat, A. Cerezo, A. K. Petford-Long, G. D. W. Smith, P. H. Clifton, R. L. Martens, and T. F. Kelly, Acta Mater. **49**, 4005 (2001).
[24]O. Kirakami, H. Sato, Y. Shimada, F. Sato, and M. Tanaka, Phys. Rev. B **56**, 13849 (1997).
[25]R. Allenspach, M. Stampanoni, and A. Bischof, Phys. Rev. Lett. **65**, 3344 (1990).
[26]O. Šipr, S. Polesya, J. Minár, and H. Ebert, J. Phys.: Condens. Matter **19**, 446205 (2007).
[27]B. Pauwels, G. Van Tendeloo, W. Bouwen, L. T. Kuhn, P. Lievens, H. Lei, and M. Hou, Phys. Rev. B **62**, 10383 (2000).
[28]V. S. Stepanyuk, D V. Tsivlin, D. Sander, W. Hergert, and J. Kirschner, Thin Solid Films **428**, 1 (2003).